Design and Validation of a Lower - Limb Haptic Rehabilitation Robot

Alexander R. Dawson-Elli, Peter G. Adamczyk, Member, IEEE

Abstract - Present robots for investigating lower-limb motor control and rehabilitation focus on gait training. An alternative approach is to focus on restoring precursor abilities such as motor adaptation and volitional movement, as is common in upper-limb robotic therapy. Here we describe NOTTABIKE, a one degree-offreedom rehabilitation robot designed to probe and promote these underlying capabilities. A recumbent exercise cycle platform is powered with a servomotor and instrumented with angular encoders, force-torque sensing pedals, and a wireless EMG system. Virtual environments ranging from spring-mass-damper systems to novel foot-to-crank mechanical laws present variants of legreaching and pedaling tasks that challenge perception, cognition, motion planning, and motor control systems. This paper characterizes the dynamic performance and haptic rendering accuracy of NOTTABIKE and presents an example motor adaptation task to illustrate its use. Torque and velocity mode controllers showed near unity magnitude ratio and phase loss less than 60 degrees up to 10 Hz. Spring rendering demonstrated 1% mean error in stiffness, and damper rendering performed comparably at 2.5%. Virtual mass rendering was less accurate but successful in varying perceived mass. NOTTABIKE will be used to study lower-limb motor adaptation in intact and impaired persons and to develop rehabilitation protocols that promote volitional movement recovery.

Index Terms— biomechatronics, lower limb, neuromotor control, rehabilitation robotics, robot control

I. INTRODUCTION

Most information about motor control and rehabilitation has been derived from studies of upper limb reaching and manipulation. Haptic robotics have played a key role in establishing motor learning principles from experiment. The ability to control the mechanical environment of the limb and hand allows experimenters to present subjects with tasks they have not encountered previously, and then observe the processes of motor adaptation and learning. This approach has led to a set of motor control insights and guiding principles for rehabilitation intervention [1]. First, the brain can build internal models of limb dynamics [2] and multiple such models coexist or interfere in predictable ways. Second, amplifying error can accelerate motor learning [3]–[5]. Third, dynamically manipulating task success rate can optimize patient motivation [6]–[9] leading to higher self-selected work volumes. Finally,

This work was supported in part by: the University of Wisconsin-Madison Office of the Vice Chancellor for Research and Graduate Education with funding from the Wisconsin Alumni Research Foundation; the UW-Madison Institute for Clinical and Translational Research (under NIH/NCATS grant UL1TR000427); the National Center for Simulation in Rehabilitation Research

task assistance should only be applied as needed [10]–[12], not continuously. An implicit principle common to upper-limb rehabilitation approaches is volitional control [13]: movements – typically reaching – are initiated by the user; the tasks require cognitive engagement to respond to visual and mechanical stimuli; and completing the task requires a full chain of neural control including perception, cognition, planning, initiation, execution, and feedback. This circuit of afferent and efferent neural activity is thought to be important for neural plasticity [14], [15].

By contrast, approaches to lower limb rehabilitation have focused almost exclusively on cyclic tasks, especially gait and gait-like tasks. For instance, early training approaches on the Hocoma Lokomat [16] exoskeleton played back pre-recorded gait patterns to provide proprioceptive input similar to normal gait [17]. Extensions to improve the volitional engagement of these activities have included the Lokomat as well as a variety of other machines, ranging from haptic foot plates to wholelimb or single-joint exoskeletons (for excellent reviews, see [18], [19]). These systems have been used to explore different control strategies including assist-as-needed impedance control, adaptive control that responds to user success, or electromyography-driven control [18]. These strategies comport with best practices in motor rehabilitation, but the overwhelming focus on using them within a walking context leads to fundamental challenges to accessibility and therefore scalability in final application. Such problems include high device complexity (and therefore cost, space and dedicated personnel), substantial time and effort in mounting the device to the user or the user to the device, and in some cases a substantial minimum functional level of the user prior to therapy. There remains a need for solutions that are simple, easy to use, and usable early in the recovery process, while still using motor rehabilitation principles to evoke high volitional engagement.

A recumbent pedal-based robot could meet this need, building upon past [20] use of recumbent cycles and steppers. In clinical use, powered cycle ergometers such as the MOTOmed [21] and RT300 [22] are used to move subjects through cyclic motions, though without explicitly requiring volitional muscle activation. In research, pedaling backward has been shown to require a change in timing for a subset of muscles [23], [24]. Studies of split-crank pedaling [25] have shown ipsilateral

(under NIH/NICHD grant HD065690-06A1); and the U.S. National Science Foundation (grant CMMI-1830516.

A.R. Dawson-Elli is with the University of Wisconsin-Madison, Madison, WI 53706 USA (e-mail: dawsonelli@wisc.edu).

P. G. Adamczyk is with the University of Wisconsin-Madison, Madison, WI 53706 USA (e-mail: peter.adamczyk@wisc.edu).

NOTTABIKE System Overview Safety Switch Flectronics Box Instrumented Pedal Motor

Figure 1 - NOTTABIKE is a one degree-of-freedom robot used to study human motor control and to deliver rehabilitation in the lower-limb. Measurements of subject endpoint kinematics and kinetics are used by a computer controller to create virtual haptic environments.

motor coordination pattern is altered by the state of the contralateral leg [26], [27] suggesting cross-couplings between extensor and flexor muscle groups. Recent cycling research suggests skillful cycling leads to longer lasting cortical activation changes than constant speed pedaling [28]. And, experiments on the NuStep [29] recumbent stepper have demonstrated an excitatory effect of upper limb activity on lower limb EMG during rhythmic tasks [30], [31]. In hemiparetic subjects, pedaling studies have shown reduced work generation on the affected side [32], [33] but retained ability to increase force output against an increased work load when demanded [34]. Other studies indicate that it is foot force direction, rather than magnitude that is primarily affected after stroke [35]. These studies and rehabilitation approaches are frequently based on the idea that much of lower limb control is managed by subcortical neural structures that are adapted to cyclic motion [36]. But, rehabilitation that relies exclusively on cyclic motions, without compelling volitional engagement, may miss a critical step by failing to engage cortical structures that need to recover or adapt [37].

Our goal is to combine the simplicity of a pedaling system with motor rehabilitation principles gleaned from upper limb reaching, emphasizing engagement of cortical structures through volitional movements in the lower limb. As opposed to an all-at-once approach of directly emulating gait, we propose to use lower-limb reaching in different haptic environments to develop motor competency through a series of subtasks related to gait. The large forces inherent in lower limb movement prevent the direct application of upper limb reaching robots to studying motor control in the lower limb. To address this gap, we built a powered, instrumented robotic exercise cycle (NOTTABIKE) to present cognitively demanding reaching and pedaling tasks in novel haptic mechanical environments in the lower limb.

Haptic environments are important because they enable a researcher to present specific mechanical conditions to a moving limb. These environments may be designed to present conditions that the motor system has never experienced before (to study motor learning), or conditions that incentivize specific aspects of motor control that need to be improved (for rehabilitation). In the upper limb, environments such as viscous curl [2], haptic tunnels [38], and error augmentation [39] have been used to derive motor learning principles. NOTTABIKE was created to facilitate the study of similar haptic environments in the lower limb. A few haptic lower limb robots have been implemented before [40]–[42], but none in the context of pedaling-like movement.

NOTTABIKE Drivetrain Detail

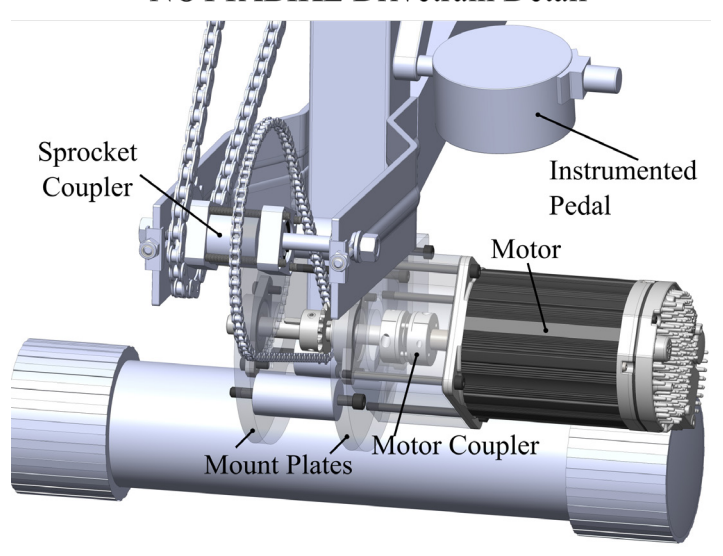


Figure 2 - Two-stage mechanical drivetrain of NOTTABIKE. The drivetrain provides efficient power transfer between the user, who interacts through the pedals, and the industrial servomotor.

System Architecture

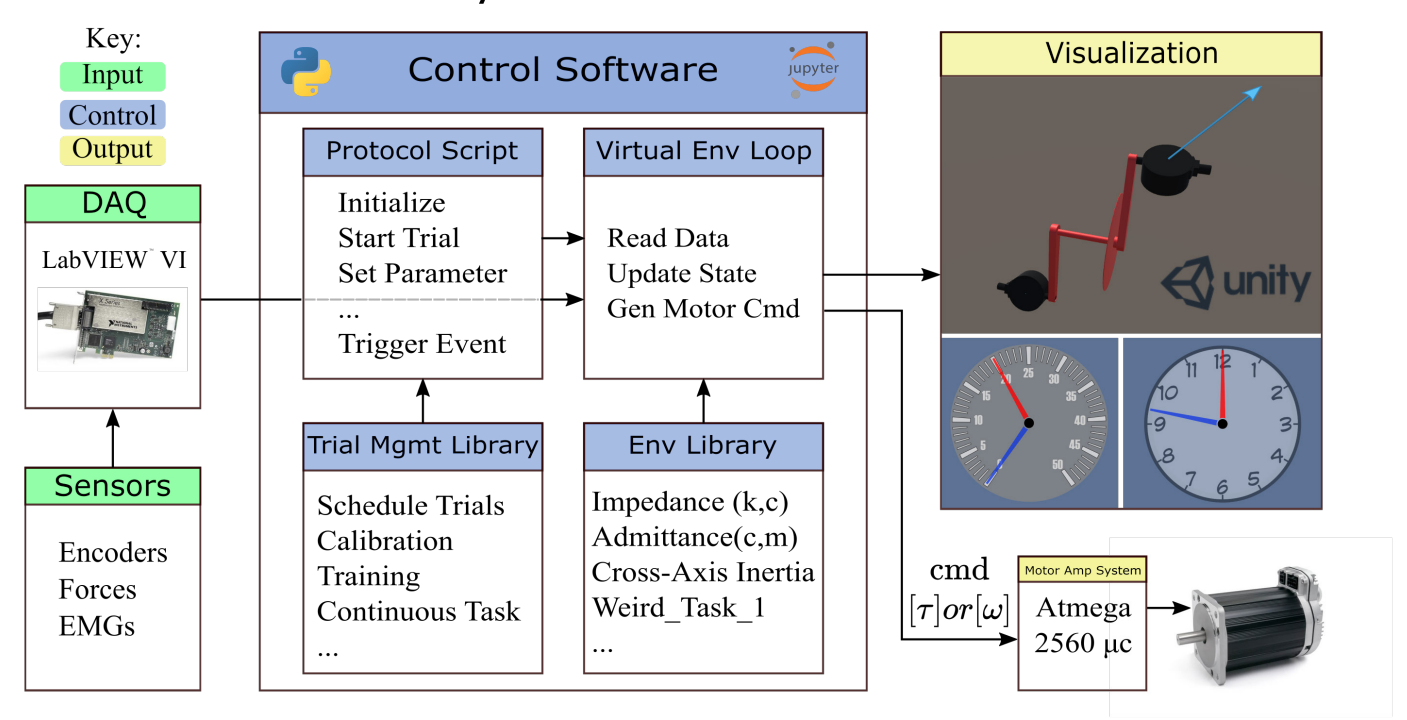


Figure 3 – Schematic representation of the system architecture. Measurements from encoders, force sensors, and EMG sensors are read through a LabVIEW Virtual Instrument at 1000Hz and are streamed to a virtual environment loop running in (Python) Jupyter Notebook at 100Hz. The state of the robot is updated, and a command torque or velocity is calculated based on the currently selected haptic environment from the Environment Library. Experiments may be designed and executed in the Protocol Script using tools from the Trial Management Library. Outputs are then sent to the motor amplifier and a visualization program to provide performance feedback to the user.

This paper describes the design and performance of the NOTTABIKE platform. The system is built on a recumbent exercise cycle frame and has a single actuated degree-of-freedom powered by an industrial servomotor. An array of sensors record foot reaction forces and moments, crank and pedal kinematics, and muscle electromyographic (EMG) activity, which are used to compute state and control the motor. We evaluate the performance of the system using ramp-input, step-input and frequency response tests, and demonstrate human interaction with multiple haptic environments. We conclude with a demonstration of using NOTTABIKE to probe adaptation to haptic rendering of different spring stiffnesses. A preliminary version of this work has been reported [43].

II. METHODS

The Neuromotor Optimization Testbed for Training in Atypical Behavior-Inducing Kinetic Environments (NOTTABIKE; Figure 1) is based on a recumbent exercise cycle platform, but its purpose is not pedaling exercise. Rather, it is a one degree-of-freedom haptic leg rehabilitation robot designed to render customized virtual environments defining the foot-to crank mechanical interaction. The recumbent posture is intended to enable early intervention following neuromotor injury, before ambulatory capacity is reestablished. The haptic environments are intended to demand active motor exploration and volitional engagement in non-cyclic tasks like targeted leg reaching, foot force control or manipulation of a dynamic system, and to provide proprioceptive afferent neural activity to encourage

neural plasticity. The goals are to explore motor control in volitional leg movements, characterize deficits and capacity in performance and motor learning in impaired and unimpaired persons, and develop therapeutic exercises that promote targeted improvement in these deficits.

The NOTTABIKE system is designed to render impedanceand admittance-based haptic environments. Mechatronic subsystems include a high-performance industrial servomotor, a custom drivetrain, and kinetic and kinematic sensors. A custom multi-threaded software framework enables setting up and running rehabilitation exercises and human motor control experiments. The following sections present the mechatronic design, control architecture, and system performance characterization in a series of electromechanical and human interaction tests.

A. Mechatronic Design – Drivetrain and Communication

The frame of the robot is a retrofitted recumbent stationary bicycle. The frame consists of square steel tube construction with an adjustable padded seat and bilateral hand holds with integral grip-actuated safety switches.

The power subsystem is based on a brushless DC servomotor with integrated high-bandwidth velocity and torque mode controllers (ClearPath CPM-MCVC-3441S-RLN, Teknic Inc., Victor, NY, USA). The motor can provide peak torque of 13 Nm at the spindle, and peak assistive power of 350 W. This motor was chosen for its high torque density and low peak velocity (840RPM). A 75 VDC, 350 W continuous power

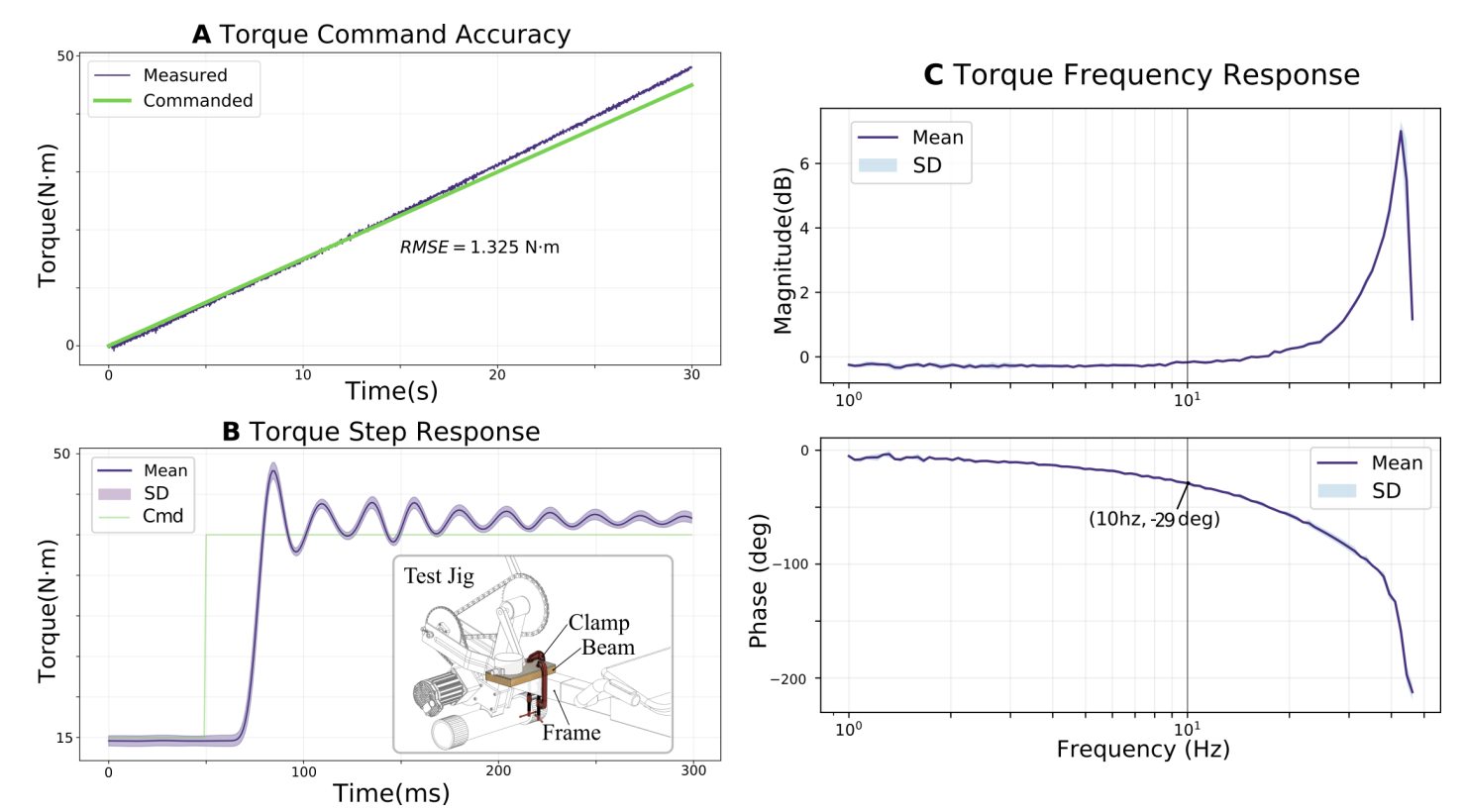


Figure 4 – (A) Torque command accuracy to a ramp function over a 30 second trial. (B) Average torque step response from a baseline torque of 15 Nm to a target torque of 40 Nm. Rise time was determined to be 29 ms. (B inset) Pedal fixation arrangement for torque response testing. Torque was controlled by the motor's internal circuitry only, and measured with the pedal load cell. (C) Average frequency response function to a torque chirp input baseline torque was 20Nm with 10Nm peak-to-peak magnitude. Notable features include magnitude of approximately unity and phase lag less than 29 degrees up to 10 Hz.

supply was used (IPC-5, Teknic Inc., Victor, NY, USA) to source power during assistive operation, and an 800W regeneration clamp and power resistor dissipates power during resistive operation (Applied Motion Products, Watsonville, CA, USA).

The drivetrain transfers power between the motor and the crank. It consists of a motor mount, a two-stage chain transmission, and a bottom-bracket and crank assembly (Figure 2). This design was selected over alternative approaches because high drivetrain efficiency and backdrivability are required for accurate impedance-based haptic renderings. The motor is attached to the steel frame by a custom aluminum mounting bracket which is pinch fit to the frame to allow freedom for chain tensioning. A 10mm diameter steel driveshaft rests between bearing blocks and connects to the motor through a rotary shaft coupler. A two-stage chain-and-sprocket reduction transfers power from the drive shaft to the pedal crank. The overall gear ratio between the rotation of the motor and the crank is 3128:320 or 9.775:1.

Communication to the integrated controller on the servomotor is achieved through Pulse Width Modulation (PWM) of control lines. A dedicated microcontroller (Atmega 2560, Atmel Corp. San Jose, CA, USA) converts command packets received over a serial communication port into 8 kHz PWM control signals. The motor controller interprets these PWM signals as velocity or torque commands. The motor's integrated controller may be placed into either velocity or torque mode via commands sent over USB from the host computer.

The motor system has several safety features that protect the user from encountering excessive torque or velocity. First, software limits on torque and velocity are set on the motor's embedded controller (nominal settings for this application are equivalent to 70 Nm and 30 RPM at the crank). Second, we installed two safety switches, one under each hand, that must both be depressed for the motor to receive power from the power supply. If at any time one of these safety switches is released, power to the motor is cut and the system enters a passive damped state facilitated by the motor back-EMF.

B. Mechatronic Design - Sensors

The robot is instrumented with sensors to measure forces and moments at the pedal interface, angular rotations of the crank and pedals, and Electromyographic (EMG) activity of the user's leg muscles. These data are sampled by a 16-bit data acquisition (DAO) card (PCIE-6343, National Instruments, Austin, TX, USA) and are used for High-Level control (see section C) and logged for analysis through a desktop computer (Windows 10 operating system, Microsoft Corp., Redmond WA). Foot endpoint forces, moments, and pedal angular positions are measured by instrumented pedals (I-Crankset, Sensix, Poitiers, France). Each pedal contains a six-component force-torque load cell with internal amplification and signal conditioning. Maximum simultaneous force measurement is 250 N in the F_x (lateral) and F_v (anterior) directions and 2000 N in F_z. (normal to the pedal) - more than adequate for experimentation in healthy subjects. Optical quadrature encoders on each pedal

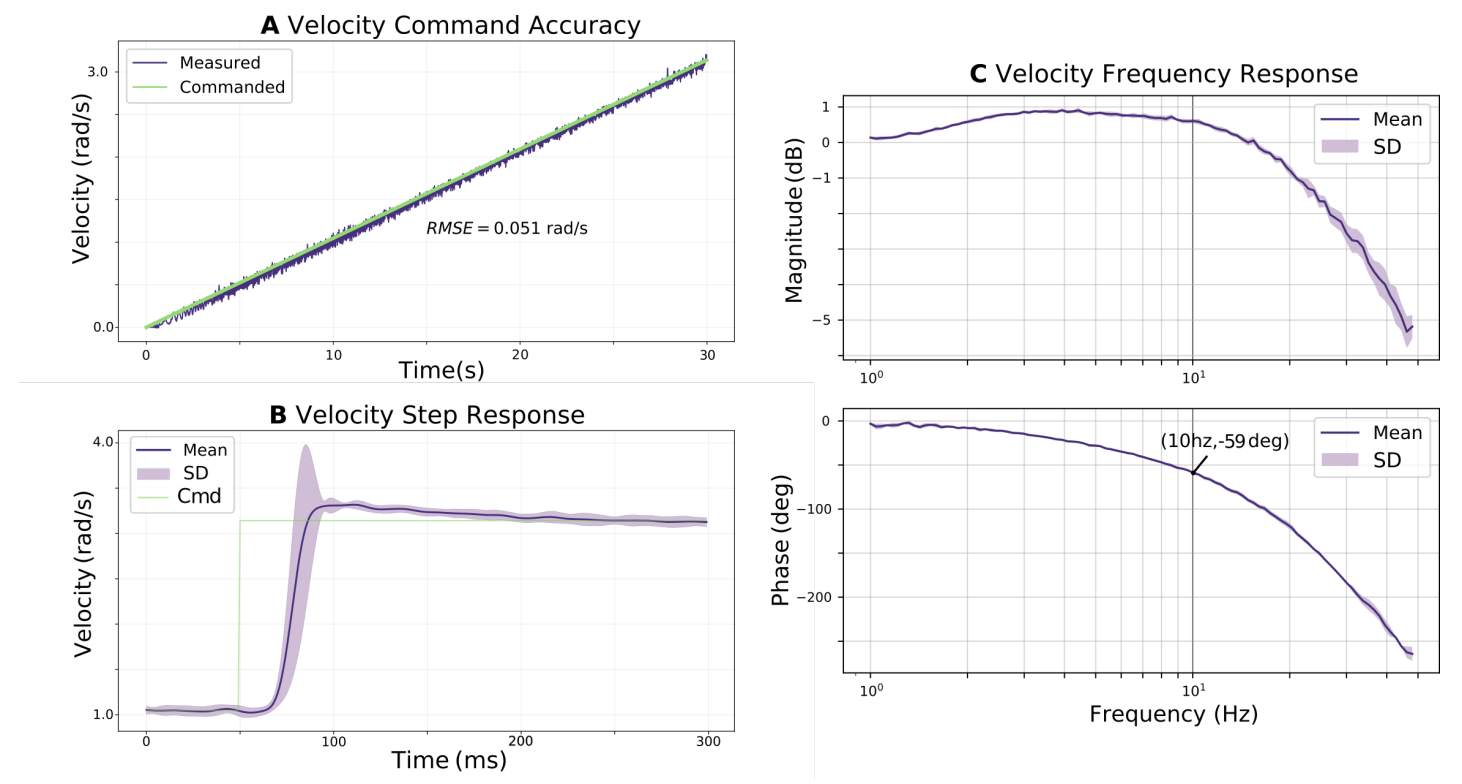


Figure 5 - (A) Velocity command accuracy to a ramp function over a 30 second trial. (B) Average velocity step-response from a baseline velocity of 1.0 rad/s to a target velocity of 3.14 rad/s (30 RPM). Rise time was determined to be 36 ms. (C) Average frequency response function to a velocity chirp input. Notable features include magnitude ratio within 1dB (12%) of unity and phase lag less than 59 degrees up to 10Hz.

axis generate 20000 counts per revolution. Crank kinematics are measured with a magnetic quadrature encoder ring fixed to the left crank and a reader fixed to the frame, which generate 24000 counts per revolution. The amplified analog signals from each pedal and quadrature channels are collected in a junction box and output over a VHDCI cable into the DAC card. A wireless EMG system (Trigno Avanti Research+, Delsys, Natick, MA, USA) records up to 16 channels of EMG and relays them onto analog lines for synchronized recording on the DAC. EMG System relay delay is 42 ms.

C. Control and Software Architecture

The control system of the robot is implemented with a cascaded architecture across multiple processors connected by communication interfaces. A high-level control law rendering a specified haptic environment runs on a desktop computer at 100Hz. From that virtually rendered haptic environment, a torque or velocity is calculated and commanded to a low-level processor integrated into the servomotor. The servomotor controller then performs closed-loop control on the specified variable using internal collocated sensors. This architecture combines the benefits of the high-performance timing of a microcontroller with the flexibility of programming a desktop computer.

The software system is comprised of several modules. Data is acquired from the DAQ card using a dedicated LabVIEW virtual instrument (VI). These data are streamed to a Python control software responsible for facilitating experiment execution and haptic environment rendering. Finally, data are

streamed from the Python control software to a visualization program and the low-level servomotor controller. (Figure 3). The LabVIEW VI collects data at 1 kHz using a hardware clock on the DAC. The three angle encoders (crank and both pedals), forces, and EMG data are buffered into an array for transmission at 100 Hz to the Python controller over an internal UDP communications socket.

Data from LabVIEW are received by the virtual environment loop and parsed to update the state of the robot. High-level control laws are defined within the Environments library to specify desired crank output parameters from present system state. Two haptic rendering approaches are used under different circumstances – impedance- and admittance-based rendering. Impedance-based rendering measures robot kinematics and controls motor torque, while admittance-based rendering does the converse. Impedance-based environments excel at rendering springs, while admittance based environments are better at rendering masses [44]. In general, high-level control laws take the form of any constraint between a measured and a commanded variable. This generic architecture enables many potential targeted and precise learning environments. (see Discussion section).

After data are received and the system state is updated, the motor command is calculated based on the currently enabled virtual environment and is sent to the motor where collocated control is performed using the motor's integrated controller and sensors. Collocated control is preferred over non-collocated control for stability when there exists compliance between the motor and the load. Additional state information may be sent to the visualization loop to provide the subject with biofeedback.

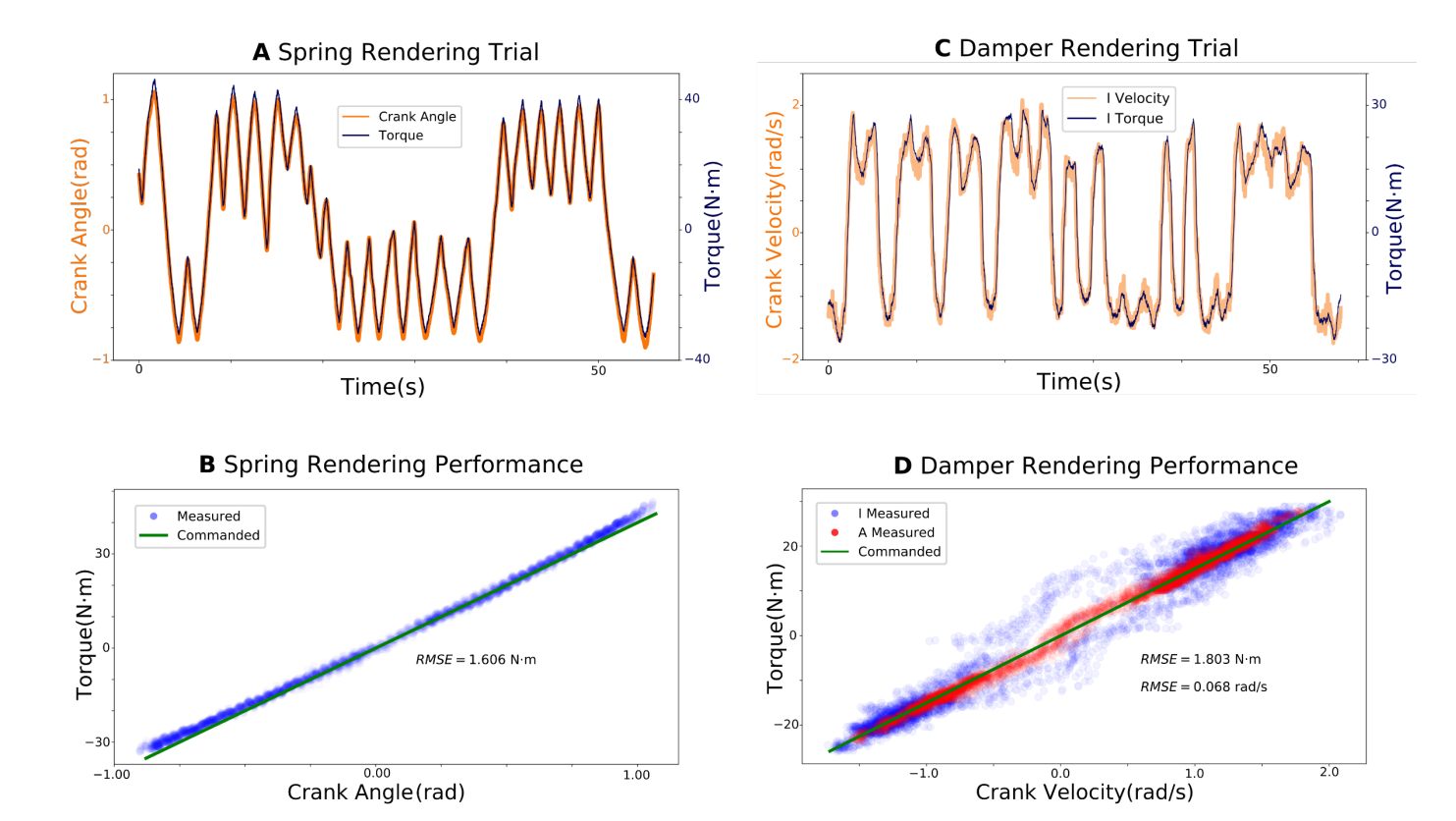


Figure 6 – (A) Crank angle and torque over time during an impedance-based haptic rendering of a spring (k = 40 Nm/rad). (B) Regression between measured torque and measured crank angle for the spring of part A. (C) Crank velocity and crank torque vs. time during an impedance-based rendering of a damper ($c = 15 \text{ Nm(rad/s)}^{-1}$) (D) Regression between measured torque and crank velocity for both impedance- and admittance-based haptic damper renderings.

Visual feedback is provided by two-dimensional or three-dimensional user interfaces built with Unity Engine (Unity Technologies, San Francisco, CA, USA). Two-dimensional visual feedback is displayed on a computer monitor directly in front of the subject. 2D widgets convey information about position, velocity, and other trial conditions using intuitive displays such as a clock face or speedometer dial. Other information may also be displayed, including dials to indicate system parameters on subsequent trials, vectors to indicate desired vs. actual force direction and magnitude, graphs of muscle EMG envelope, and scores to increase motivation and decrease subject slacking [45]–[47].

Experiments may be performed through a protocol scripting interface in Python running within the Jupyter Notebook environment. We developed a variety of tools for specifying, tuning, and recording trials, which are contained within the Trial Management library. The protocol script sends messages to the virtual environment loop to change system behavior. An example of such a script might enable recording, set a system parameter to a particular value, wait for an end condition such as time or accomplishment of a task goal, and then increment the trial. This design enables complex and precise experimental protocols to be specified and executed.

D. Evaluation - Machine Performance Testing

We conducted a series of tests to characterize device performance, including quantifying torque and velocity measurement accuracy, step-input response, and frequency response. Investigating the performance limits of the device allowed us to benchmark its capabilities against other lower limb robotic systems.

We fashioned a jig to lock the rotation of the crank during testing. We made a cantilever beam of steel plate backed by a wooden board and clamped it perpendicular to the robot frame in line with the right pedal (Figure 4B inset). We placed the right pedal in contact with the beam so it could measure the force between the beam and the pedal face. The reaction force supplied by the beam prevented the crank from rotating in the backward direction.

We first evaluated the torque command accuracy of the robot. We sent a ramp torque command from 0 Nm to 30 Nm over a period of 30 seconds to the motor controller. We calculated RMS error between commanded and measured torque (Figure 4A). It is important to note that the sensor feedback from the pedal was not used to control torque: torque was controlled independently by the motor's integrated controller using onboard collocated sensors, and performance was evaluated using the torque measured separately through the instrumented pedals. Thus, from the perspective of the high-level control law, the motor may be treated as a torque source, and the response may be viewed as an open-loop response. It was therefore important to establish congruence between the torque command and torque measurement.

We next evaluated torque step response. We applied a baseline torque (15 Nm) to assure that the pedal face was firmly in contact with the cantilever beam. We then applied a step command (40 Nm) to the servomotor and measured the

resulting forces on the pedal. We recorded 10 trials and plotted the average response (mean \pm SD) (Figure 4B). We evaluated performance in each trial with rise time (time between when the command was issued 50ms into the trial and 100% of final value) and settling time (time to settle within 5% of the final value) criteria.

We next evaluated torque frequency response. We created a linear torque chirp signal with a peak-to-peak magnitude of 10 Nm and an offset of 20 Nm. The initial frequency was set to 0.05 Hz and the terminal frequency was 50 Hz, with a duration of 90 s.

Next, we calculated the frequency response function (FRF) for torque control. We calculated magnitude ratio as the quotient of the RMS torque output over the RMS torque command. For each evaluated frequency in the chirp signal, we used a half-second (500 sample) window centered at the time when the test frequency was commanded. We also calculated phase using the lag at maximum cross-correlation between output and input signals within the same window. We performed this analysis on each of the 10 trials, and we plotted the magnitude and phase as a function of frequency (mean \pm SD) (Figure 4C).

To evaluate velocity command accuracy, we applied a speed ramp command starting at 0 rad/s and ending at 3.14 rad/sec (30 RPM) after 30 seconds. We measured crank position from the encoder and used the central difference method to estimate crank velocity. We applied a 50 Hz bandwidth linear IIR filter and calculated RMS error between the commanded and measured velocities (Figure 5A). It is important to note that the sensor feedback from the crank encoder was not used to control velocity: velocity was controlled independently by the servomotor's integrated controller, and performance was evaluated using the crank encoder.

We also evaluated the velocity step response between a baseline velocity of 1.05 rad/s and a final velocity of 3.14 rad/s. We averaged 10 trials and plotted the resulting velocity \pm SD (Figure 5B). We evaluated response time and settling time using 100% final value and 5% settling error criteria, as in the torque step test.

Finally, we calculated the frequency response function (FRF) for velocity control. We applied 10 linear chirps sequentially. Each chirp signal had duration 90 seconds, starting frequency 0.05Hz, terminal frequency 50Hz, and amplitude 2.09 rad/s with a baseline of 1.05rad/s. We calculated and plotted the velocity FRF using the same approach described in the torque section (Figure 5C).

E. Evaluation – Human Interaction Testing

We conducted a series of tests to quantitatively evaluate the ability of the robot to render different impedance- and admittance-based haptic environments during human machine interaction. Since the robot is instrumented with both kinematic and kinetic sensors, we can render a haptic environment with one sensor and assess environment accuracy with the other. We evaluated human interaction with an impedance-based spring, an impedance-based damper, and an admittance-based damper, with parameters that fall within a range useful for neuromuscular investigation and therapeutic intervention. The interaction testing setup was visually identical to that demonstrated in Figure 1. Research was performed under the

oversight of the University of Wisconsin-Madison Health Sciences IRB submission ID# 2016-1279-CP001. Informed consent was received for all human subjects involved in testing. These tests establish the suitability of NOTTABIKE for the study of motor control and rehabilitation.

An impedance-based spring measures the crank angle θ and commands a motor torque τ computed from a mathematical representation of a torsional spring, $\tau = k\theta$. A single subject interacted with three impedance-based spring environments with stiffnesses of $k = \{10, 40, 70\}$ Nm/rad for one minute each. The subject was told to move freely back and forth within each environment. We recorded the measured crank angle and the torque calculated from the instrumented pedals for each condition. We plotted the measured crank angle and measured torque over time in Figure 6A for k = 40 Nm/rad to demonstrate their correspondence visually. We also used least-squares linear regression to estimate the apparent external stiffness of the rendered virtual spring. (Figure 6B).

An impedance-based damper relates the measured crank velocity ω to commanded motor torque τ through the mathematical expression $\tau = c\omega$. The controller estimates crank velocity using a backward difference method and a 50Hz linear IIR filter. We evaluated and analyzed damping coefficients $c = \{5, 15, 25\}$ Nm(rad/s)⁻¹ in the same fashion as the impedance-based spring (Figures 6C and 6D).

An admittance-based damper relates torque applied externally to the pedals to commanded servomotor velocity through the equation $\omega = \frac{\tau}{c}$. In this case, the controller estimates torque from the instrumented pedals and commands angular velocity ω . We evaluated the admittance-based damper for $c = \{5, 15, 25\}$ Nm(rad/s)⁻¹. We used measured crank kinematics as validation data. We estimated velocity with the central difference method and applied a 50 Hz linear filter. We plotted the regression between measured force and measured velocity on the same plot as the impedance-based trial to facilitate direct comparison (Figure 6D). Only the c = 15 Nm(rad/s)⁻¹ trial was plotted, for visual clarity. A summary of the results of human testing is provided in Table 1.

III. RESULTS

For the torque ramp test, error between the commanded (open loop) and measured torque was 1.33 Nm RMS. Error was negligible at low torque, increasing to a modest overestimate at higher torque values (roughly 6% at 45 N command). The torque step rise time was 29 ± 1 ms (mean \pm SD), and the settling time was 125 ± 50 ms. Torque frequency response did not exhibit magnitude roll-off within the 50 Hz command bandwidth (limited due to 100 Hz command update frequency). A key result from the torque frequency analysis is that the magnitude ratio is unity up to 10 Hz with only 29 degrees phase lag.

For the velocity ramp test, error between commanded (open loop) and measured signals was 0.051 rad/s RMS, with uniform accuracy throughout the commanded range (0-30 rad/s). The velocity step rise time was 36 ± 7 ms and settling time was 90 \pm 35 ms. Magnitude ratio was within 1 dB of unity at all frequencies below 10 Hz, with less than 59 degrees phase lag. Results of the haptic rendering tests during human interaction are displayed in Table 1. All three springs rendered within 1%

of the desired spring constant, with RMS torque error less than 2 Nm within the range tested (roughly -50 to +70 Nm). Damping environments performed similarly on average when rendered using impedance-control and admittance-control, with larger torque variability using impedance-control. Impedance-controlled dampers rendered within 6% of the desired damping constant, with RMS torque error less than 3.4 Nm. Admittance-controlled dampers performed within 2.5% of the desired damping constant, with RMS velocity error less than 0.1 rad/s.

IV. DISCUSSION

A. Interpretation of Results and System Design

The results presented here confirm that the torque, velocity, and haptic rendering performance of NOTTABIKE are suitable for studying motor control and rehabilitation in the lower limb. Haptic environments for human interaction testing are rendered within a few percent of desired parameters, across a wide range of stiffness and damping. Both the torque and velocity control modes have near unity magnitude ratio and small phase loss up to 10 Hz, exceeding the bandwidth of other lower limb rehabilitation robots [48]. For context, humans' ability to track unpredictable stimuli deteriorates around 1-2 Hz [49], and the control bandwidth of the human leg is roughly 2 Hz [2].

The phase loss is likely attributable to a time lag resulting from drive train compliance. The source of the compliance is the deflection of transmission mounting forks under tension and backlash from residual slack in the drive train. The time lag can most readily be seen in the torque and velocity step response plots, in the time between when torque or velocity is commanded and when the robot responds. This time is 16ms and 18ms respectively. Thus, in this respect, the performance of the robot is most limited by the drive train.

At first glance, there appears to be a discrepancy between the torque step and chirp responses. While the step response shows a gain slightly greater than unity, the chirp response shows magnitude below 0 dB. This may be explained by two factors. First, the chirp response and step response were conducted at different torque amplitudes, and the slight nonlinearity in the pedal measurements (see Figure 4a) could cause different amplitude measurements. Second, the measurements are experimental in nature, so slow drift in the strain gauges or motor behavior (e.g. due to temperature) could cause the two results to differ slightly.

From the torque frequency and step responses it appears the robot resonates around 40 Hz. This may be an artifact of the cantilever beam setup used to evaluate the frequency response. The amplification of the velocity before the magnitude roll-off observed in the velocity chirp response may be due to a resonance of the pedal mass connected through the compliance of the drivetrain. The authors do not believe this negatively impacts machine performance or safety in any practical manner as the peak amplification is 1dB or 12% amplification. None of these features adversely affect the rendering capability of the robot within the frequency range necessary for the study of motor learning.

A limitation of our analysis is that the human's effect on the torque and velocity controllers was not directly analyzed in the frequency domain. Humans contribute mass which will lower system bandwidth, and human joint impedance can vary over two orders of magnitude depending on level of muscular co-contraction[50] and limb posture, making the experimental determination of the human's effect on a controller difficult to determine. As such, the human's effect on the controller likely contributed to the tracking error in the human interaction tests. Because the time domain and regression results fell within our desired performance limits, this analysis was not undertaken.

In addition to the stiffness and damping performance analyzed above, the third component of rendering haptic environments is inertia — the relationship between torque and angular acceleration, as in the traditional mass-spring-damper system. NOTTABIKE can render inertia, but assessing the performance of inertia rendering proved difficult because the only available estimate of angular acceleration is from double differentiation of the crank angle signal. The resulting acceleration signal is very noisy, so we did not use it to assess inertia rendering quantitatively. Qualitatively, subjects interacting with simulated inertias report that they are "smooth" and "feel like normal pedaling" when combined with light damping. Subjects were able to perceive easily the difference among inertias of $I = \{5, 10, 40\}$ kg-m².

The design of the control system is unusual for a robotic system, in that it includes a Windows desktop computer in the control loop. The desktop computer cannot perform high-bandwidth motor control, so it was also crucial to incorporate the integrated servo controller. Thus, parameters updated relatively slowly by the desktop computer's virtual environment model (100 Hz) produce motor commands (torque or velocity) that are tightly controlled at much higher bandwidth by the servomotor controller. This design decision had important benefits. Programming on a desktop with a high-level language enables rapid control law prototyping, easy data storage and sophisticated data visualization for biofeedback – here, through the Unity gaming engine. It also opens the possibility of creating control paradigms that incorporate data from patient history rather than just the current system state, for example by using patient specific models and machine learning approaches.

B. Importance of the Approach

NOTTABIKE was built to enable different styles of lower-limb rehabilitation, based on rehabilitating volitional control of the leg in goal-directed movements rather than task-specific gait training. The use of haptic environments provides a means to create demanding motor tasks and incentivize them in a controlled way, by tuning task difficulty and success rates for optimal challenge and motivation [8]. Task incentives in the

Table 1: Assessing The Quality of Haptic Rendering

Haptic	Target parameter	Rendered	Correlation	RMSE
env		parameter	coefficient	
I-spring	k = 10 Nm/rad	10.09	0.9945	0.92 Nm
	k = 40 Nm/rad	39.82	0.9987	1.60 Nm
	k = 70 Nm/rad	69.35	0.9990	1.96 Nm
I-	$c = 5 \text{ Nm(rad/s)}^{-1}$	5.32	0.9866	1.22 Nm
damper	$c = 15 \text{ Nm}(\text{rad/s})^{-1}$	14.98	0.9811	1.80 Nm
	$c = 25 \text{ Nm}(\text{rad/s})^{-1}$	23.83	0.9568	3.37 Nm
A-	$c = 5 \text{ Nm}(\text{rad/s})^{-1}$	5.08	0.9970	0.100 rad/s
damper	$c = 15 \text{ Nm}(\text{rad/s})^{-1}$	15.32	0.9973	0.068 rad/s
	$c = 25 \text{ Nm}(\text{rad/s})^{-1}$	25.55	0.9950	0.079 rad/s

form of minimal encouragement toward volitional activity [12] or as a firm requirement for task completion [51] have been successful in the upper limb. These precedents suggest that explicitly rewarding volitional control of a targeted motor task may lead to increased motor learning and neuromotor recovery.

. Haptic rendering may be combined with visual feedback to create multimodal learning environments. The addition of task-relevant visual feedback can increase motivation by making the task demands more understandable and intuitive[52]. NOTTABIKE uses a series of 2 and 3 dimensional widgets to provide real-time performance information about task parameters to the subject(Figure 3). Training effects arise when the human uses this information to reduce error and learn new control strategies. Figure 7 demonstrates subjects using visual feedback to reach a target angle against haptically rendered springs of different stiffnesses.

NOTTABIKE uses a recumbent posture to separate the targeted tasks of motor coordination from the confounding demands of upright balance and weight support. The recumbent posture could also enable robotic rehabilitation earlier in the process of recovery from injuries such as stroke compared to treadmill training or exoskeleton walking. The approach is intended to redevelop motor coordination through a progressive series of subtasks, rather than all at once. It is envisioned as an early intervention to prepare the motor system for later task-specific gait and balance training.

NOTTABIKE also embodies an inversion of the usual paradigm for lower-limb rehabilitation robots. Exoskeletal robots are often designed to control many kinematic degrees of freedom, often with minimal measurement of interaction forces with the user [53]. The underlying assumption in such cases is that the movement itself is rehabilitative and the robot can drive it with minimal response to the user [54]. In contrast, our view of rehabilitation is that only user-generated actions (forces, movements) are rehabilitative – and therefore that the primary action of the robot should be to respond to the user, not to initiate movement. Therefore sensing, not actuation, is the focus of NOTTABIKE, and the exercises it prescribes use its one degree of freedom to provide kinematic or kinetic responses to many potential inputs. The one degree-of-freedom design results in a mechanically simple device that can still create complex virtual environments that require volitional engagement and elicit motor learning.

This single degree of freedom does present the obvious limitation that movement can only occur along a circular path; therefore NOTTABIKE cannot create true multidimensional haptic environments like viscous curl [2]. However, force-driven control can still occur along dimensions that are kinematically constrained. For instance, forward motion of the crank can be controlled by the magnitude of lateral force produced by the user. Environments may be arbitrarily precise to target specific changes. For example, left dorsiflexor modulation can be targeted by controlling crank velocity in proportion to EMG activation of the left tibialis anterior muscle at specific ranges of crank angle. Or, bilateral abductor control can be targeted by controlling crank angle in proportion to symmetric abductor force measured at the pedals. Environments such as these may enable the exploration of

Spring Adaptation Demonstration

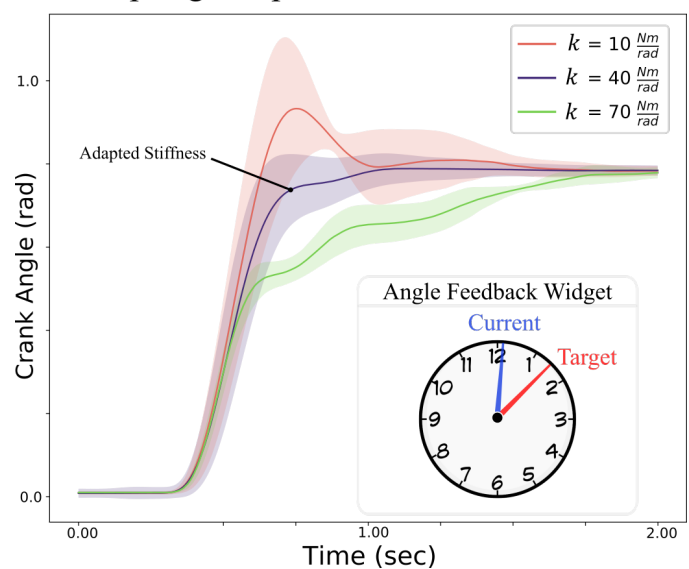


Figure 7– Demonstration of motor adaptation to springs of different stiffnesses on NOTTABIKE in a single subject under visual feedback of performance with a clock widget (inset). 50 reaching trials were performed: 80% with the medium stiffness k=40 Nm/rad and 10% catch trials to each of $k=\{10,70\}$ Nm/rad. Subject attempted to reach 45deg (.78rad) in the least time possible.

lower limb motor synergies, believed to be important in pathological movement after stroke [55]. NOTTABIKE may even render Virtual environments with nonphysical properties that can only be realized through simulation, such as negative mass that accelerates backward when it is pushed forward. The novelty of such environments is critical for motor-learning studies because of the importance of testing activities which do not have a basis in the test subject's past experience.

Another limitation of a single degree of freedom robot is that it cannot elicit kinematic movement deviations as an indicator of motor adaptation or motor learning. Thus, path errors and spatial convergence cannot be observed. However, there remains a great deal of information available about motor performance in the force, position, velocity and time domains, which may be used to quantify task performance. For example, the overshoot and undershoot shown in Figure 7 provide strong evidence of imperfect adaptation to the soft and stiff virtual springs, respectively, due to training focused on the medium stiffness spring. The amount of a movement completed within the initial submovement is also a key indicator of motor adaptation [46]. Thus, methods from psychophysics based on time and movement extent can be adapted to elucidate findings on motor control.

C. Future Directions

NOTTABIKE provides an effective platform to train and test a variety of motor tasks that could be useful for basic science in motor control as well as rehabilitation. Our first study will investigate motor adaptation in the lower limb through a series of reaching tasks in haptic spring, damper, and mass environments with healthy subjects. This will allow us to establish normative metrics for adaptation in the lower-limb, and evaluate the extent to which principles established in the

upper-limb [1] generalize. We will also investigate the time course of long-term motor learning in healthy subjects through repeated testing experiments across multiple days and weeks. We will further investigate the ability to train novel tasks that require new motor patterns, using novel environments such as half-reversed pedaling (reversing the sign of the torque generated by one leg), and inverse-curl fields (setting crank velocity in proportion to lateral force).

Following these and other motor experiments in health subjects, we will compare the capacity for motor adaptation in a clinical population of patients recovering from stroke. We anticipate that these tests may lead to methods for quantifying deficit and differentiating those individuals with a greater or lesser capacity for improvement (responders vs. non-responders). We will further investigate how training on NOTTABIKE can improve motor function in a clinical population, using those tasks most successful in provoking motor learning in movements targeted to overcome common deficits due to stroke.

V. CONCLUSION

NOTTABIKE can render both impedance- and admittance-based haptic environments with accuracy and responsiveness that are useful for the study of human coordination and the delivery of rehabilitative therapy. Future work using this robot will explore motor adaptation in the lower limb in intact subjects and haptic environments with therapeutic value to a clinical population. The ability to test goal-directed movements in the lower limb will enable comparison of how motor learning principles and techniques for the lower limb relate to those established previously in the upper limb.

REFERENCES

- D. J. Reinkensmeyer, J. L. Emken, and S. C. Cramer, "Robotics, Motor Learning, and Neurologic Recovery," *Annu. Rev. Biomed. Eng.*, vol. 6, no. 1, pp. 497–525, 2004, doi: 10.1146/annurev.bioeng.6.040803.140223.
- [2] R. Shadmehr and F. Mussa-Ivaldi, "Adaptive representation of dynamics during learning of a motor task," *J. Neurosci.*, vol. 14, no. 5, pp. 3208–3224, May 1994, Accessed: Aug. 12, 2011. [Online]. Available: http://www.jneurosci.org/content/14/5/3208.abstract.
- [3] F. Abdollahi et al., "Error augmentation enhancing arm recovery in individuals with chronic stroke a randomized crossover design," Neurorehabil. Neural Repair, p. 1545968313498649, 2013, Accessed: Oct. 17, 2016. [Online]. Available: http://nnr.sagepub.com/content/early/2013/08/07/1545968313498649.ab stract
- [4] J. L. Patton, M. E. Stoykov, M. Kovic, and F. A. Mussa-Ivaldi, "Evaluation of robotic training forces that either enhance or reduce error in chronic hemiparetic stroke survivors," *Exp. Brain Res.*, vol. 168, no. 3, pp. 368–383, 2006, Accessed: May 17, 2013. [Online]. Available: http://link.springer.com/article/10.1007/s00221-005-0097-8.
- [5] F. Abdollahi et al., "Error Augmentation Enhancing Arm Recovery in Individuals With Chronic Stroke: A Randomized Crossover Design," Neurorehabil. Neural Repair, vol. 28, no. 2, pp. 120–128, Feb. 2014, doi: 10.1177/1545968313498649.
- [6] D. A. Brown, T. D. Lee, D. J. Reinkensmeyer, and J. E. Duarte, "Designing Robots That Challenge to Optimize Motor Learning," in *Neurorehabilitation Technology*, D. J. Reinkensmeyer and V. Dietz, Eds. Springer International Publishing, 2016, pp. 39–58.
- [7] D. J. Reinkensmeyer and S. J. Housman, "'If I can't do it once, why do it a hundred times?': Connecting volition to movement success in a virtual environment motivates people to exercise the arm after stroke," in 2007 Virtual Rehabilitation, 2007, pp. 44–48, Accessed: Aug. 01,

- 2016. [Online]. Available:
- http://ieeexplore.ieee.org/xpls/abs_all.jsp?arnumber=4362128.

 [8] J. E. Duarte and D. J. Reinkensmeyer, "Effects of robotically modulating kinematic variability on motor skill learning and motivation," *J. Neurophysiol.*, vol. 113, no. 7, pp. 2682–2691, 2015, Accessed: Aug. 01, 2016. [Online]. Available: http://jn.physiology.org/content/113/7/2682.abstract.
- [9] J. E. Duarte and D. J. Reinkensmeyer, "The Real-World Challenge Point Hypothesis: Predicting the consequences of challenge for unsupervised motor training," presented at the Biomechanics and Neural Control of Movement 2016, Mt. Sterling, Ohio, USA, Jun. 2016.
- [10] S. Srivastava et al., "Assist-as-Needed Robot-Aided Gait Training Improves Walking Function in Individuals Following Stroke," IEEE Trans. Neural Syst. Rehabil. Eng. Publ. IEEE Eng. Med. Biol. Soc., vol. 23, no. 6, pp. 956–963, Nov. 2015, doi: 10.1109/TNSRE.2014.2360822.
- [11] J. L. Emken, R. Benitez, and D. J. Reinkensmeyer, "Human-robot cooperative movement training: learning a novel sensory motor transformation during walking with robotic assistance-as-needed," *J. NeuroEngineering Rehabil.*, vol. 4, no. 1, p. 1, 2007, Accessed: Aug. 01, 2016. [Online]. Available: http://jneuroengrehab.biomedcentral.com/articles/10.1186/1743-0003-4-8
- [12] E. T. Wolbrecht, V. Chan, D. J. Reinkensmeyer, and J. E. Bobrow, "Optimizing Compliant, Model-Based Robotic Assistance to Promote Neurorehabilitation," *IEEE Trans. Neural Syst. Rehabil. Eng.*, vol. 16, no. 3, pp. 286–297, Jun. 2008, doi: 10.1109/TNSRE.2008.918389.
- [13] A. A. Blank, J. A. French, A. U. Pehlivan, and M. K. O'Malley, "Current Trends in Robot-Assisted Upper-Limb Stroke Rehabilitation: Promoting Patient Engagement in Therapy," Curr. Phys. Med. Rehabil. Rep., vol. 2, no. 3, pp. 184–195, Sep. 2014, doi: 10.1007/s40141-014-0056-z.
- [14] E. Dayan and L. G. Cohen, "Neuroplasticity subserving motor skill learning," *Neuron*, vol. 72, no. 3, pp. 443–454, 2011.
- [15] B. Draganski, C. Gaser, V. Busch, G. Schuierer, U. Bogdahn, and A. May, "Neuroplasticity: changes in grey matter induced by training," *Nature*, vol. 427, no. 6972, p. 311, 2004.
- [16] "Lokomat®," *Hocoma*. https://www.hocoma.com/solutions/lokomat/ (accessed Jul. 20, 2017).
- [17] K. P. Westlake and C. Patten, "Pilot study of Lokomat versus manual-assisted treadmill training for locomotor recovery post-stroke," *J. NeuroEngineering Rehabil.*, vol. 6, no. 1, p. 18, Dec. 2009, doi: 10.1186/1743-0003-6-18.
- [18] W. Meng, Q. Liu, Z. Zhou, Q. Ai, B. Sheng, and S. (Shane) Xie, "Recent development of mechanisms and control strategies for robotassisted lower limb rehabilitation," *Mechatronics*, vol. 31, pp. 132–145, Oct. 2015, doi: 10.1016/j.mechatronics.2015.04.005.
- [19] A. J. Young and D. P. Ferris, "State of the Art and Future Directions for Lower Limb Robotic Exoskeletons," *IEEE Trans. Neural Syst. Rehabil.* Eng., vol. 25, no. 2, pp. 171–182, Feb. 2017, doi: 10.1109/TNSRE.2016.2521160.
- [20] R. G. Ranky, M. L. Sivak, J. A. Lewis, V. K. Gade, J. E. Deutsch, and C. Mavroidis, "Modular mechatronic system for stationary bicycles interfaced with virtual environment for rehabilitation," *J. NeuroEngineering Rehabil.*, vol. 11, no. 1, p. 93, Jun. 2014, doi: 10.1186/1743-0003-11-93.
- [21] Reck, "MOTOmed viva2," MOTOmed viva2. http://www.motomed.com/en/models/motomed-viva2.html (accessed Sep. 01, 2015).
- [22] "RT300 series FES powered rehabilitation therapy systems." http://restorative-therapies.com/rt300_series (accessed Sep. 01, 2015).
- [23] L. H. Ting, S. A. Kautz, D. A. Brown, and F. E. Zajac, "Phase Reversal of Biomechanical Functions and Muscle Activity in Backward Pedaling," *J. Neurophysiol.*, vol. 81, no. 2, pp. 544–551, Feb. 1999, Accessed: Jul. 24, 2015. [Online]. Available: http://jn.physiology.org/content/81/2/544.
- [24] C. C. Raasch and F. E. Zajac, "Locomotor strategy for pedaling: muscle groups and biomechanical functions," *J. Neurophysiol.*, vol. 82, no. 2, pp. 515–525, Aug. 1999, doi: 10.1152/jn.1999.82.2.515.
- [25] H. F. M. Van der Loos, L. Worthen-Chaudhari, D. Schwandt, D. M. Bevly, and S. A. Kautz, "A Split-Crank Bicycle Ergometer Uses Servomotors to Provide Programmable Pedal Forces for Studies in Human Biomechanics," *IEEE Trans. Neural Syst. Rehabil. Eng.*, vol. 18, no. 4, pp. 445–452, Aug. 2010, doi: 10.1109/TNSRE.2010.2047586.
- [26] L. H. Ting, C. C. Raasch, D. A. Brown, S. A. Kautz, and F. E. Zajac, "Sensorimotor state of the contralateral leg affects ipsilateral muscle

- coordination of pedaling," *J. Neurophysiol.*, vol. 80, no. 3, pp. 1341–1351, 1998.
- [27] L. H. Ting, S. A. Kautz, D. A. Brown, and F. E. Zajac, "Contralateral movement and extensor force generation alter flexion phase muscle coordination in pedaling," *J. Neurophysiol.*, vol. 83, no. 6, pp. 3351– 3365, 2000.
- [28] T. Tatemoto, S. Tanaka, K. Maeda, S. Tanabe, K. Kondo, and T. Yamaguchi, "Skillful Cycling Training Induces Cortical Plasticity in the Lower Extremity Motor Cortex Area in Healthy Persons," Front. Neurosci., vol. 13, 2019, doi: 10.3389/fnins.2019.00927.
- [29] "NuStep," NuStep, LLC, Oct. 24, 2016. https://www.nustep.com/ (accessed Aug. 13, 2019).
- [30] H. J. Huang and D. P. Ferris, "Neural coupling between upper and lower limbs during recumbent stepping," *J. Appl. Physiol.*, vol. 97, no. 4, pp. 1299–1308, Oct. 2004, doi: 10.1152/japplphysiol.01350.2003.
- [31] D. P. Ferris, H. J. Huang, and P.-C. Kao, "Moving the Arms to Activate the Legs:," Exerc. Sport Sci. Rev., vol. 34, no. 3, pp. 113–120, Jul. 2006, doi: 10.1249/00003677-200607000-00005.
- [32] S. A. Kautz and D. A. Brown, "Relationships between timing of muscle excitation and impaired motor performance during cyclical lower extremity movement in post-stroke hemiplegia.," *Brain*, vol. 121, no. 3, pp. 515–526, Mar. 1998, doi: 10.1093/brain/121.3.515.
- [33] D. A. Brown and S. A. Kautz, "Speed-Dependent Reductions of Force Output in People With Poststroke Hemiparesis," *Phys. Ther.*, vol. 79, no. 10, pp. 919–930, Oct. 1999, doi: 10.1093/ptj/79.10.919.
- [34] D. A. Brown and S. Kautz, "Increased workload enhances force output during pedaling exercise in persons with poststroke hemiplegia," *Stroke*, vol. 29, no. 3, pp. 598–606, 1998.
- [35] L. M. Rogers, D. A. Brown, and K. G. Gruben, "Foot force direction control during leg pushes against fixed and moving pedals in persons post-stroke," *Gait Posture*, vol. 19, no. 1, pp. 58–68, Feb. 2004, doi: 10.1016/S0966-6362(03)00009-2.
- [36] M. R. Dimitrijevic, Y. Gerasimenko, and M. M. Pinter, "Evidence for a Spinal Central Pattern Generator in Humans," *Ann. N. Y. Acad. Sci.*, vol. 860, no. 1, pp. 360–376, 1998.
- [37] D. J. Reinkensmeyer *et al.*, "Computational neurorehabilitation: modeling plasticity and learning to predict recovery," *J. Neuroengineering Rehabil.*, vol. 13, no. 1, p. 42, 2016, doi: 10.1186/s12984-016-0148-3.
- [38] E. H. F. van Asseldonk, M. Wessels, A. H. A. Stienen, F. C. T. van der Helm, and H. van der Kooij, "Influence of haptic guidance in learning a novel visuomotor task," *J. Physiol.-Paris*, vol. 103, no. 3, pp. 276–285, May 2009, doi: 10.1016/j.jphysparis.2009.08.010.
- [39] F. Abdollahi et al., "Arm control recovery enhanced by error augmentation," in 2011 IEEE International Conference on Rehabilitation Robotics, Jun. 2011, pp. 1–6, doi: 10.1109/ICORR.2011.5975504.
- [40] H. Schmidt, S. Hesse, R. Bernhardt, and J. Krüger, "HapticWalker—a novel haptic foot device," ACM Trans. Appl. Percept. TAP, vol. 2, no. 2, pp. 166–180, 2005.
- [41] J. F. Veneman, R. Kruidhof, E. E. G. Hekman, R. Ekkelenkamp, E. H. F. Van Asseldonk, and H. van der Kooij, "Design and evaluation of the LOPES exoskeleton robot for interactive gait rehabilitation," *IEEE Trans. Neural Syst. Rehabil. Eng. Publ. IEEE Eng. Med. Biol. Soc.*, vol. 15, no. 3, pp. 379–386, Sep. 2007, doi: 10.1109/TNSRE.2003.818185.
- [42] M. Girone, G. Burdea, M. Bouzit, V. Popescu, and J. E. Deutsch, "A Stewart Platform-Based System for Ankle Telerehabilitation," *Auton. Robots*, vol. 10, no. 2, pp. 203–212, Mar. 2001, doi: 10.1023/A:1008938121020.
- [43] A. R. Dawson-Elli and P. G. Adamczyk, "NOTTABIKE a haptic robot for studying motor control and applying rehabilitation in the lower limb," presented at the International Society of Biomechanics, Calgary, Aug. 2019.
- [44] C. Parthiban and M. Zinn, "Performance and stability limitations of admittance-based haptic interfaces," in 2018 IEEE Haptics Symposium (HAPTICS), San Francisco, CA, Mar. 2018, pp. 58–65, doi: 10.1109/HAPTICS.2018.8357153.
- [45] D. J. Reinkensmeyer, O. Akoner, D. P. Ferris, and K. E. Gordon, "Slacking by the human motor system: computational models and implications for robotic orthoses," *Conf. Proc. Annu. Int. Conf. IEEE Eng. Med. Biol. Soc. IEEE Eng. Med. Biol. Soc. Conf.*, vol. 2009, pp. 2129–2132, 2009, doi: 10.1109/IEMBS.2009.5333978.
- [46] M. Casadio and V. Sanguineti, "Learning, Retention, and Slacking: A Model of the Dynamics of Recovery in Robot Therapy," *IEEE Trans. Neural Syst. Rehabil. Eng.*, vol. 20, no. 3, pp. 286–296, May 2012, doi:

- 10.1109/TNSRE.2012.2190827.
- [47] J. L. Emken, R. Benitez, A. Sideris, J. E. Bobrow, and D. J. Reinkensmeyer, "Motor Adaptation as a Greedy Optimization of Error and Effort," *J. Neurophysiol.*, vol. 97, no. 6, pp. 3997–4006, Jun. 2007, doi: 10.1152/jn.01095.2006.
- [48] J. L. Emken, J. H. Wynne, S. J. Harkema, and D. J. Reinkensmeyer, "A robotic device for manipulating human stepping," *IEEE Trans. Robot.*, vol. 22, no. 1, pp. 185–189, Feb. 2006, doi: 10.1109/TRO.2005.861481.
- [49] I. D. Loram, H. Gollee, M. Lakie, and P. J. Gawthrop, "Human control of an inverted pendulum: Is continuous control necessary? Is intermittent control effective? Is intermittent control physiological?," *J. Physiol.*, vol. 589, no. 2, pp. 307–324, 2011, doi: 10.1113/jphysiol.2010.194712.
- [50] N. Hogan, "Controlling impedance at the man/machine interface," in Proceedings, 1989 International Conference on Robotics and Automation, Scottsdale, AZ, USA, 1989, pp. 1626–1631, doi: 10.1109/ROBOT.1989.100210.
- [51] E. B. Brokaw, T. Murray, T. Nef, and P. S. Lum, "Retraining of interjoint arm coordination after stroke using robot-assisted timeindependent functional training," *J. Rehabil. Res. Dev.*, vol. 48, no. 4, pp. 299–316, 2011.
- [52] H. Huang, S. L. Wolf, and J. He, "Recent developments in biofeedback for neuromotor rehabilitation," *J. NeuroEngineering Rehabil.*, vol. 3, no. 1, p. 11, Jun. 2006, doi: 10.1186/1743-0003-3-11.
- [53] G. Chen, C. K. Chan, Z. Guo, and H. Yu, "A Review of Lower Extremity Assistive Robotic Exoskeletons in Rehabilitation Therapy," *Crit. Rev. Biomed. Eng.*, vol. 41, no. 4–5, 2013, doi: 10.1615/CritRevBiomedEng.2014010453.
- [54] A. Esquenazi et al., "Clinical Application of Robotics and Technology in the Restoration of Walking," in *Neurorehabilitation Technology*, D. J. Reinkensmeyer and V. Dietz, Eds. Cham: Springer International Publishing, 2016, pp. 223–248.
- [55] Hayes Cruz Theresa and Dhaher Yasin Y., "Evidence of Abnormal Lower-Limb Torque Coupling After Stroke," Stroke, vol. 39, no. 1, pp. 139–147, Jan. 2008, doi: 10.1161/STROKEAHA.107.492413.